Energy & Environmental Science

Accepted Manuscript

ROYAL SOCIETY OF CHEMISTRY

www.rsc.org/ees

Energy & Environmental Science

RSCPublishing

ARTICLE

Design of hydrothermally-stable dawsonite-based sorbents in technical form for CO_2 capture†

O. Martin, M. Hammes, S. Mitchell, and J. Pérez-Ramírez*

Cite this: DOI: 10.1039/x0xx00000x

Received 00th January 2014,
Accepted 00th January 2014

DOI: 10.1039/x0xx00000x

www.rsc.org/

Among prospective CO_2 capture sorbents, systems based on the formation of dawsonite ($XAlCO_3(OH)_2$, X = Na, K) have received limited attention, despite displaying attractive reversible uptakes under hydrothermal conditions. Here, we combine a detailed understanding of the nanoscale structural transformations, originating the higher total and net capacity of potassium dawsonite-based systems with respect to those based on sodium dawsonite or hydrotalcite, with the mesoscale challenges faced in translating this promising performance to industrially-relevant, mm-sized shaped forms such as extrudates. In comparison with the extrusion of bulk precursors, the impregnation of alumina bodies uniquely enables the attainment of shaped sorbents of non-negligible porosity and of variable potassium loading and distribution. Examination of internal cross-sections of the sorbents by scanning electron microscopy coupled with energy dispersive X-ray analysis and focused ion beam cutting clearly discerns the critical relation between these parameters and the loss of mechanical integrity due to internal stresses caused by the growth of needle-like dawsonite crystals upon carbonation. The latter can be avoided through the strategic application of common pore formers and binders, resulting in stable performance over multiple cycles without compromising the net capacity, while favourably reducing kinetic limitations observed over densely-packed extrudates. These results unambiguously demonstrate the importance of adopting a multiscale approach for the development of improved CO_2 capture technologies.

1 Introduction

The expected global increase in CO_2 emissions from coal-fired power plants in the next decades[1] demands more sustainable methods of carbon capture, utilisation, and storage (CCUS).[2–4] In the short term, post-combustion capture strategies are favoured over pre-combustion or oxyfuel ones, since their implementation can be facilitated by retro-fitting to existing infrastructure, as will be first demonstrated on industrial scale in Saskatchewan, Canada, this year.[5] Apart from satisfying a number of general criteria, including to be non-toxic, cheap, and to exhibit fast carbonation/regeneration kinetics and a selective high uptake, an ideal sorbent for post-combustion application must also be hydrothermally-stable.[6] Aqueous amines are applied in the state-of-the-art wet scrubbing process to remove CO_2 from natural gas or H_2.[7] However, the corrosive nature of the amines and the high energy requirement for their regeneration have sparked widespread efforts to develop alternatives,[8,9] especially physi-/chemisorbents in solid form.[10–12]

Many groups have studied amine-functionalised supports for overcoming the drawbacks of liquid amines,[13,14] but their preparation is not straightforward. Nanoporous physisorbents like metal-organic frameworks,[15,16] zeolites,[17,18] and carbon-based[10,19] materials, can exhibit high CO_2 capacities. However, they often suffer from poor selectivity and material degradation in humid atmospheres.[20,21] On the other hand, cheap chemisorbents such as CaO-based systems, which selectively remove CO_2 with high uptakes,[22–24] require elevated carbonation (873–973 K) and regeneration temperatures (>1223 K). Although a fluidised bed process has been demonstrated, the prevention of sorbent deactivation due to particle sintering or attrition remains a challenge.[25,26] Furthermore, while well-known hydrotalcite-like materials reveal stable uptakes,[27,28] their capacities, although enhanced in humid atmospheres, are generally lower than those of other chemisorbents.[29]

Institute for Chemical and Bioengineering, Department of Chemistry and Applied Biosciences, ETH Zurich, Vladimir-Prelog-Weg 1, CH-8093 Zurich, Switzerland. E-mail: jpr@chem.ethz.ch; Fax: +41 44 633 1405.

† Electronic supplementary information (ESI) available: Fig. S1–7. See DOI: 10.1039/b000000x/

Systems based on sodium and potassium bicarbonate also function in the presence of water (eqn (1)) and have been investigated as low-temperature sorbents (<373 K).[30,31] In this case, supported systems are normally applied to enhance the carbonation and regeneration kinetics by maximising the adsorption surface. However, the interaction of the alkali metals

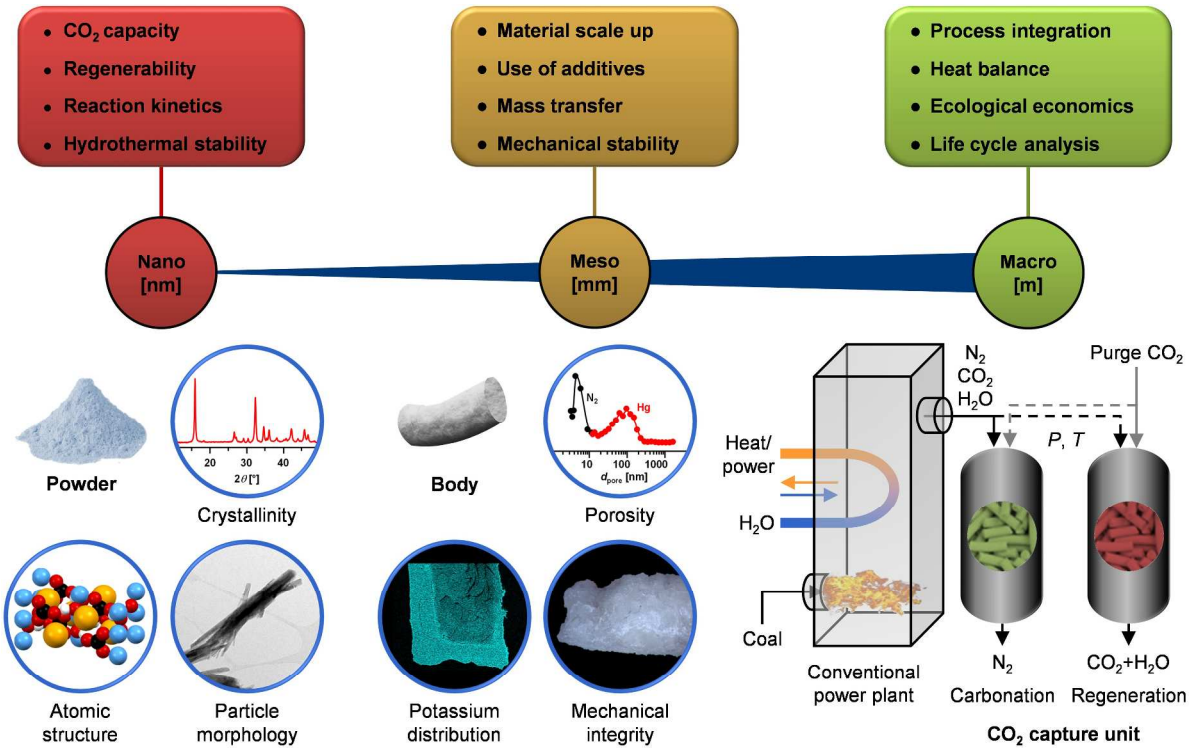

Fig. 1 Multi-scale considerations (upper panels) which need to be bridged in the development of dawsonite-based sorbents for post-combustion CO_2 capture, and relevant properties which can be optimised (lower panels). Of these, the often-neglected transition from nano- to mesoscale requires the identification of appropriate strategies to form mechanically-stable shaped bodies and suitable descriptors for their performance.

with the support can influence the performance, as was observed in the case of γ-Al_2O_3 where the formation of dawsonite phases ($XAlCO_3(OH)_2$, X = Na, K) led to a gradual reduction of the CO_2 capacity, since the temperature applied for the regeneration of the bicarbonate sorbent (<473 K) was insufficient to decompose the dawsonite phase.

On the other hand, the reversible formation of dawsonite following thermal decomposition ("memory effect", eqn (2)), first demonstrated by Stoica *et al.*[33,34] upon treatment in aqueous alkali carbonate solutions and later extended to gas–solid systems by Walspurger *et al.*,[35] yields stable CO_2 uptakes over multiple cycles at elevated temperatures and pressures. According to eqns (1) and (2), the theoretical capture efficiency of dawsonite-based systems (10 mmol g^{-1}) would be twice that of bicarbonates in terms of the monovalent cation utilisation. Consequently, the application of dawsonite materials could be conceived under either post-combustion (15 mol.% CO_2, 0.1 MPa) or pre-combustion (35 mol.% CO_2, 3.0 MPa) conditions, particularly if the water necessary for the latter strategy could be introduced through adjustment of the preceding water-gas shift reaction.

$$(Na,K)_2CO_3 + CO_2 + H_2O \leftrightarrows \underset{\text{(bicarbonate)}}{2(Na,K)HCO_3} \quad (1)$$

$$(Na,K)AlO_2 + CO_2 + H_2O \leftrightarrows \underset{\text{(dawsonite)}}{(Na,K)AlCO_3(OH)_2} \quad (2)$$

In order to rationalise the design of improved CO_2 capture sorbents, it is indispensable to bridge multiple scales spanning from the atomic understanding (nanoscale) to the process of scale up (mesoscale), and the integration of the capture unit into the power plant (macroscale), as depicted in Fig. 1 for the case of post-combustion. However, despite the strongly intercorrelated implications for the performance, surprisingly few studies have considered the development of shaped CO_2 sorbents.[36–38] Understanding the manufacture and function of these technical mm-sized bodies (*i.e.*, granules, extrudates, *etc.*) is essential for any industrial process since the synthesis methods may differ widely from those used to prepare powders at laboratory scale, and thus it might not be possible to extrapolate the insights gained from the study of the latter to their structured counterparts.[39]

Herein, the enhanced performance of potassium dawsonite with respect to sodium dawsonite and hydrotalcite-based sorbents is demonstrated by comparative evaluation of the CO_2 uptake under wet carbonation conditions. Subsequently, different strategies are investigated to prepare extruded

potassium dawsonite systems with variable alkali metal loading and distribution. The occurrence and impact of compositional and morphological changes upon cyclic carbonation–regeneration is revealed through characterisation by XRD, N_2 sorption, Hg intrusion, and electron microscopic techniques coupled with appropriate preparation methods. Finally, the application of additives is explored to enhance the mechanical stability of the shaped sorbents.

2 Experimental

2.1 Sorbent preparation

All reagents applied for the sorbent synthesis were purchased from Alfa Aesar and had a purity >98%. Potassium (K-DW), sodium (Na-DW), and ammonium (NH_4-DW) dawsonite powders were synthesised by the coprecipitation of aqueous solutions of the respective ammonium or alkali carbonate $(NH_4)_2CO_3$, K_2CO_3, or Na_2CO_3 (2 M) and of $Al(NO_3)_3{\cdot}9H_2O$ (1 M) in a vigorously stirred tank at 333 K. The resulting slurries were maintained at a pH of 8.0 in the case of NH_4-DW or 9.3 in the cases of K-DW and Na-DW, respectively. After stirring for 2 h, the solid precipitate was isolated by filtration, washed extensively with deionised water, and dried in static air for 12 h at 338 K. The high surface area γ-Al_2O_3 ($S_{BET} > 400$ m^2 g^{-1}) utilised in this study was derived by calcination of the as-synthesised NH_4-DW in static air at 823 K (5 K min^{-1}) for 2 h. A high surface area (171 m^2 g^{-1}) hydrotalcite (HT) with a molar Mg/Al ratio of 3 was prepared as a reference sorbent by a previously reported method.[40] Accordingly, an aqueous solution of $Mg(NO_3)_3{\cdot}6H_2O$ (0.75 M) and $Al(NO_3)_3{\cdot}9H_2O$ (0.25 M) was titrated with a basic solution containing NaOH (1 M) and Na_2CO_3 (1 M) in a vigorously stirred tank at pH 10 and 303 K. The resulting slurry was filtered, washed, and dried as described above.

The strategies evaluated to attain technical dawsonite-based sorbents are fully described in the Results and discussion. Briefly, these included: (*i*) the extrusion of calcined bulk K-DW (coded B)) or mixed K(NH_4)-DW (coded $B_{diluted}$) materials, (*ii*) the impregnation of γ-Al_2O_3 with K_2CO_3 either by mixing in the paste prior to extrusion (termed paste impregnation, PI) or by subsequent wet (coded WI) or dry (coded DI) impregnation of the γ-Al_2O_3 extrudates. In the case of impregnation, potassium loadings of 27 wt.% (coded $_{high}$) and 13 wt.% (coded $_{low}$) were targeted, equivalent to the bulk or mixed materials, respectively. A mixer torque rheometer (Caleva) was used to determine the amount of water required to form an extrudable paste depending on the particular formulation. Where additives were applied to enhance the mechanical stability and the pore volume of the shaped body, including an attapulgite clay binder (10 wt.%, Fluorochem) and a corn starch pore former (10 wt.%, Agrana Stärke), they were also introduced at this stage. In the case of paste impregnation, the required amount of K_2CO_3 was dissolved in the water necessary for structuring, prior to mixing with the γ-Al_2O_3 powder. The paste was homogenised by intensive mixing and subsequently formed into extrudates using a single-screw extruder (Caleva). All materials were hardened by calcination at 823 K (2 K min^{-1} heating ramp) for 2 h in static air. In the case of the starch-containing samples, the organic additive was burnt off by a staged calcination program in an air flow (500 ml min^{-1}) with isothermal steps of 2 h at 443, 523, and 823 K (1 K min^{-1}). Wet impregnation of the calcined γ-Al_2O_3 extrudates was undertaken by stirring in a K_2CO_3 solution (0.6 M) for 12 h. Excess water was subsequently removed by rotary evaporation, before the extrudates were freeze-dried under vacuum and recalcined as detailed above. For dry impregnation, the calcined γ-Al_2O_3 extrudates were degassed at 373 K for 12 h prior to the dropwise addition of the aqueous K_2CO_3 solution, the amount of which was adjusted to the pore volume of the solid determined by mercury intrusion. Finally, the dry-impregnated bodies were dried at 338 K in static air for 12 h and recalcined as described above. The as-prepared sorbents are termed 'fresh' throughout the manuscript.

2.2 Characterisation

The contents of K, Na, Mg, and Al in the solids were determined by ICP-OES (inductively coupled plasma optical emission spectroscopy) using a Horiba Ultima2 instrument. Before analysis the samples were dissolved by heating in HCl (12 M) at 353 K for 12 h. X-ray diffraction (XRD) was measured in an X'Pert Pro MPD from PANalytical using Ni-filtered Cu-Kα radiation ($\lambda = 0.1542$ nm) with an angular size of 0.05° and a counting time of 8 s per step. Thermogravimetry was measured with a Mettler Toledo TGA/DSC STARe microbalance. Analyses were performed in N_2 (60 ml min^{-1}) ramping the temperature from 303–1173 K (5 K min^{-1}). N_2 isotherms at 77 K were measured using a Quadrasorb SI Quantachrome instrument, after degassing the samples for 6 h in vacuum at 423 K. The total surface area was determined by the BET method. Hg intrusion was performed with a Micromeritics Autopore IV in the pressure range 0.0035–418 MPa using a contact angle of 140º and an equilibration time of 10 s. Samples were degassed *in situ* prior to analysis. TEM (transmission electron microscopy) images of the gently crushed extrudates were acquired with a FEI Tecnai F30 microscope operated at 300 kV following dispersion on carbon-coated copper grids. To characterise the internal organisation of the sorbent, individual extrudates were embedded in resin (LR White), sanded to the desired position, trimmed with a microtome to achieve a flat surface, and coated with carbon (2 nm) to avoid charging. SEM (scanning electron microscopy) imaging and EDX (energy dispersive X-ray) mapping of the resulting extrudate cross-sections was conducted using a FEI Quanta 200 F microscope operated at 10 kV or 30 kV, respectively. Focused ion beam scanning electron microscopy (FIB-SEM) images were acquired with a Zeiss NVision 40 instrument using energy selective backscattered electron detection (2 kV).

2.3 Sorbent testing

Carbonation–regeneration experiments were conducted in a homemade fixed-bed reactor (12.8 mm i.d.) using high-purity carbon dioxide, nitrogen and argon gases (≥99.995%, Pangas/Linde). The sorbent (5 g) was loaded into the reactor in powder (200–400 µm sieve fraction) or extrudate (ca. 2 mm in diameter by 6 mm in length) form, resulting in bed heights of ca. 5 cm. Deionised water was continuously injected into the top of the reactor *via* a syringe pump. All downstream lines were heated to 453 K to avoid condensation. The outlet gas was analysed by a quadrupole mass spectrometer (MS) OmniStar GSD 301 (Pfeiffer Vacuum).

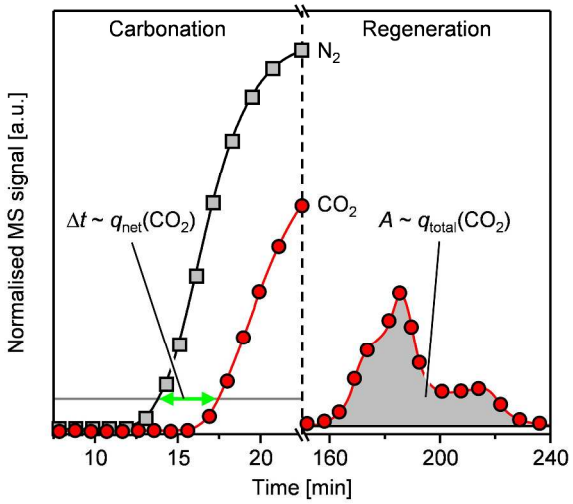

Fig. 2 N_2 (*m*/*z* 28) and CO_2 (*m*/*z* 44) signals at the reactor outlet during carbonation (left). The net CO_2 capacity is determined from the temporal difference in the breakthrough curves at 10% of the equilibrium signal (grey line). The total CO_2 capacity is calculated from the amount of CO_2 evolved during sorbent regeneration (right). Conditions of carbonation: 473 K, 3.0 MPa, H_2O:CO_2 = 1; regeneration: 773 K, 5 K min^{-1}, 3.0 MPa, Ar.

Prior to testing, the sorbent bed was activated at 573 K for 1 h (heating rate: 5 K min^{-1}) in argon at atmospheric pressure. Each capture cycle consisted of two steps: (*i*) carbonation at 473 K, 3.0 MPa with an equimolar mixture of H_2O:CO_2:N_2:Ar (total flow = 100 ml min^{-1}) for 1.5 h, and (*ii*) regeneration by heating to 773 K (5 K min^{-1}) at the same pressure under flowing argon, after reaching the maximum temperature the sorbent bed was cooled to 473 K again.

The net capacity, $q_{net}(CO_2)$, was derived from the temporal difference (Δt) in the breakthrough of N_2 and CO_2 (see Fig. 2, left) according to eqn (3):

$$q_{net}(CO_2) = \Delta t\, F(CO_2)\, m_{sorbent}^{-1} \quad (3)$$

where $F(CO_2)$ is the molar inlet flow of CO_2 and $m_{sorbent}$ the mass of sorbent used.

The total capacity, $q_{total}(CO_2)$, was determined from the amount of CO_2 released during regeneration (see Fig. 2, right) according to eqn (4):

$$q_{total}(CO_2) = A(CO_2)\, f_c\, m_{sorbent}^{-1} \quad (4)$$

where $A(CO_2)$ is the integrated CO_2 signal and f_c the calibration factor determined from the decomposition of known amounts of $KHCO_3$.

All experiments were repeated at least three times. The average uncertainty of the CO_2 uptake was estimated as 7% by an error propagation calculation over the entire dataset. However, for the sake of clarity only a single error bar is shown in each figure. The temperature-programmed sorption of CO_2 was undertaken in the same reactor. In this case, after activating the sorbent (2 g) the reactor was cooled to the starting temperature (303 K). The mass signal of *m*/*z* 44 (representing CO_2) was stabilised before starting the water injection. Then the temperature was ramped from 303 K to 673 K (5 K min^{-1}) at 0.1 MPa, H_2O:CO_2:N_2 = 5:5:90 (total flow = 100 ml min^{-1}). The reactant concentrations were reduced to ensure the complete vaporisation of water under the selected conditions. The impact of the CO_2 atmosphere on the regeneration of the carbonated sorbent was evaluated by treating the as-synthesised material (13 g) for 1 h at 773 K (5 K min^{-1}) at a pressure of 3.0 MPa of pure CO_2 in an autoclave. The sorbent was subsequently isolated by rapidly cooling under flowing CO_2.

3 Results and discussion

3.1 Comparative properties of dawsonite-based sorbents

The dawsonite-based systems were initially characterised in powder form to determine the impact of the alkali metal (Na-DW *versus* K-DW) and of the process conditions. A hydrotalcite-based system (HT), representing the established benchmark of hydrothermally-stable medium-temperature sorbents,[12] was compared for reference under equivalent conditions. Herein, the capture capacity was assessed through cyclic carbonation–regeneration experiments, applying a feed of CO_2, H_2O, N_2, and Ar in a molar ratio of 1:1:1:1 at 473 K and 3.0 MPa during the carbonation step. The net (or working) capacity ($q_{net}(CO_2)$), represents the amount of CO_2 which can be fixed by the sorbent in dynamic mode until its breakthrough is detected. Complementarily, the total capacity ($q_{total}(CO_2)$), a commonly cited parameter in carbon capture research, expresses the maximum amount of CO_2 stored under equilibrium conditions. It is important to note that the total capacity is rarely fully exploited, since technical separation columns are usually not operated under equilibrium conditions.[41]

Comparison of the net CO_2 capacity over consecutive cycles, revealed that one carbonation and regeneration was required before reaching a constant value, which was approximately 60% higher for K-DW than for Na-DW or HT (Fig. 3a). In terms of total capacity, significantly higher values were achieved over the dawsonite-based sorbents ($q_{total}(CO_2)$ = 3.06 and 2.29 mmol g^{-1} for K-DW, Na-DW, respectively), illustrating their huge potential compared with the hydrotalcite-derived system ($q_{total}(CO_2)$ = 0.49 mmol g^{-1}). This can be explained by comparison of the phase changes induced upon carbonation and regeneration, which are summarised in Fig. 3c. The low efficiency of mixed Mg-Al

oxides, which normally does not exceed a total capacity of 1 mmol g^{-1} in unpromoted forms,[11,12,42] stems from the fact that only minor reconstruction of the hydrotalcite phase occurs during carbonation under these conditions (Fig. 3b). Consequently, the observed uptake primarily relates to the interaction of CO_2 with basic MgO sites on the external surface.[43,44] In contrast, extensive recrystallisation of the parent materials ($XAlCO_3(OH)_2$, X = Na, K) is achieved upon carbonation of the fresh dawsonite-based systems, corresponding to a 30% utilisation of the alkali metal, which is 10-times superior to that of Mg in the HT system.

The much higher net capacity of Na-DW than K-DW in the first cycle (Fig. 3a) is consistent with the formation of a highly crystalline sodium dawsonite phase (Fig. 3b) upon carbonation of the fresh sorbent. Both the Na-DW and K-DW phases fully

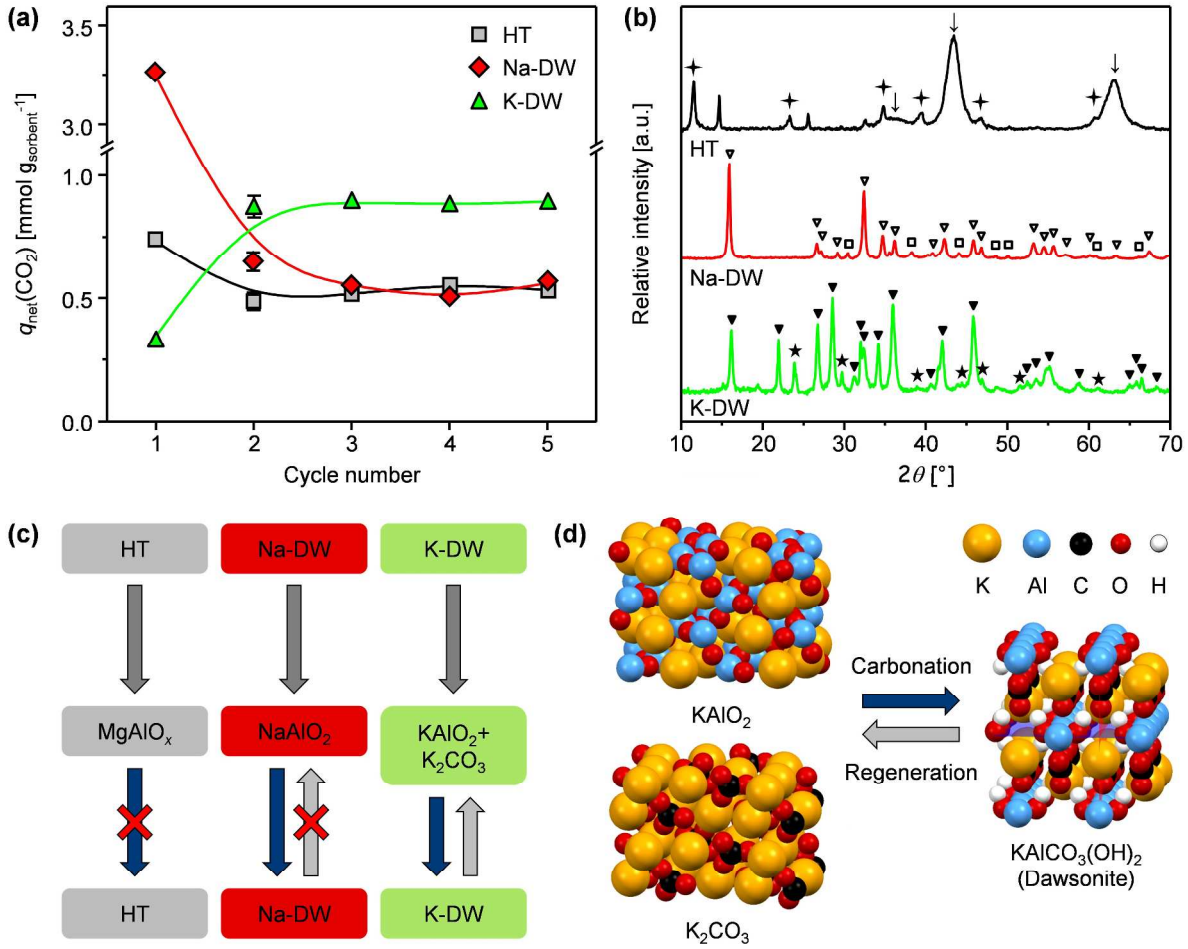

Fig. 3 (a) Net CO_2 capacity of the K-DW, Na-DW, and HT powders in sequential cycles under the conditions detailed in Fig. 2. (b) XRD patterns of the sorbents isolated after the 1st carbonation. Marked reflections were identified according to the JCPDS reference patterns: (▽) $NaAlCO_3(OH)_2$ (83-1291), (□) Na_2CO_3 (86-287), (▼) $KAlCO_3(OH)_2$ (21-979), (★) $K_2(Al_2O(OH)_6)$ (76-455), (✦) $Mg_6Al_2CO_3(OH)_{16}{\cdot}4H_2O$ (22-700), and (↓) MgO (45-946). (c) Crystalline phases in the as-synthesised (top), fresh (middle), and carbonated (bottom) samples in each system. (d) Atomistic representations of the $KAlO_2$ (JCPDS 89-8451, projected along the *b*-axis) and K_2CO_3 (JCPDS 71-1466, projected along the *c*-axis) phases, which reversibly transform into K-DW (21-979, projected along the *c*-axis) upon carbonation.

decompose upon regeneration at 773 K and 3.0 MPa, resulting in mixed carbonate/oxide phases in which reflections corresponding to Na_2CO_3 or K_2CO_3 and $KAlO_2$ are visible, respectively (Fig. S1). The remaining aluminium is present as an amorphous γ-Al_2O_3 phase, believed to be in intimate contact with the alkali carbonates. The fact that, due to the presence of stable carbonate phases, the captured CO_2 is not all released during the first regeneration, which is also seen by thermogravimetric analysis (Fig. S2), implies that a minor fraction of the potential sorbent capacity is not fully exploited. Strikingly, the net capacity of the sodium dawsonite system dropped to less than one sixth of its high initial value after the first cycle. This is attributed to the lower reactivity of the Na_2CO_3 formed upon regeneration, the carbonation of which appears to be either kinetically- and/or thermodynamically-limited in comparison with that of the $NaAlO_2$ phase present in the fresh sorbent (Fig. 3c). In contrast, the reversible transition between $KAlO_2$-K_2CO_3-Al_2O_3 systems and the dawsonite phase (Fig. 3d) yield consistently high net uptakes in the K-DW based system, which favour its application for carbon capture over Na-DW and HT.

Comparatively, the mechanism of the bulk transformation to dawsonite is more complex than the predominantly surface interaction of the mixed Mg-Al oxides. As seen from the shape of the breakthrough curves (Fig. 4a), the incorporation of CO_2 into the crystal structure appears to occur in two consecutive steps at different rates: the initial steep rise of the CO_2 curve is assumed to correlate with the carbonation of the surface, whereas the subsequent step accounts for the reaction proceeding in the bulk. Furthermore, consistent with the observed formation of dawsonite at elevated pressures by Walspurger *et al.*,[35] the CO_2 uptake was significantly enhanced on increasing the total pressure from 1 to 3 MPa (Fig. 4a).

To further characterise the optimal operating window, the phase transformations in the potassium dawsonite-based sorbent (evidenced by XRD, Fig. S3) were monitored by the temperature-programmed sorption of CO_2 (at ambient pressure, Fig. 4b). After stabilising the mass signal *m/z* 44 (CO_2), the

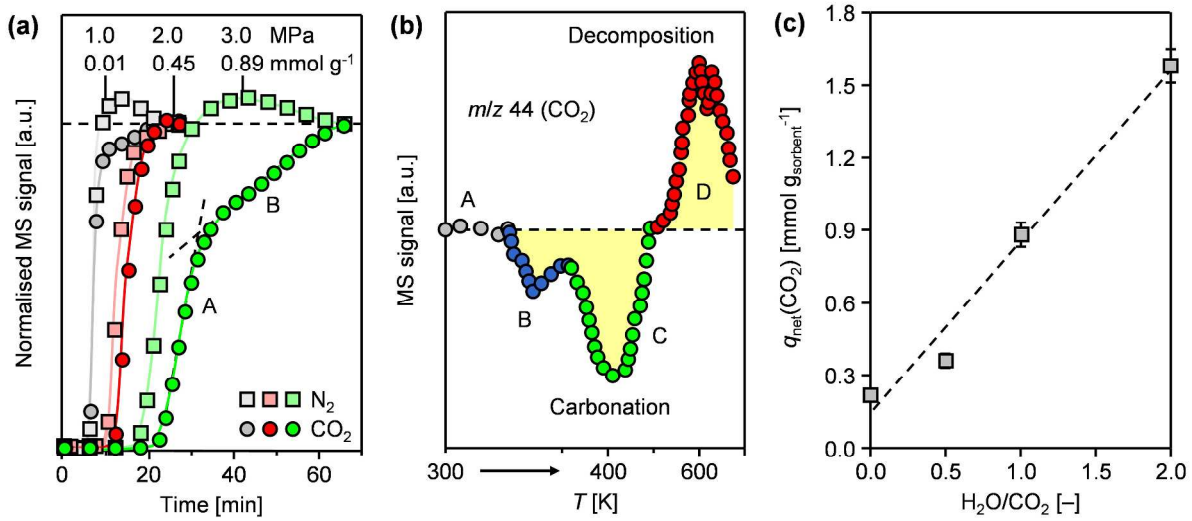

Fig. 4 Performance of the K-DW sorbent: (a) Impact of pressure on the N_2 and CO_2 breakthrough (5th cycle, conditions as detailed in Fig. 2). The larger separation at elevated pressure results in an increased net capacity (specified below the pressure). The steep initial rise in the CO_2 signal (A) is attributed to the carbonation of the particle surface, whereas the less pronounced increase (B) correlates with the bulk formation of K-DW. (b) Temperature-programmed sorption of CO_2 at 0.1 MPa, $H_2O:CO_2:N_2$ = 5:5:90, heating rate 5 K min^{-1}. Water injection began after equilibration of the MS signal (A). The uptakes and losses indicated are assigned to the formation of $KHCO_3$ (B) and to the formation (C) and subsequent degradation (D) of K-DW, respectively. (c) Variation in the net capacity with the H_2O/CO_2 feed ratio (5th cycle, conditions as detailed in Fig. 2).

continuous introduction of water at 303 K induced the formation of a potassium bicarbonate phase (Fig. S3), as expected under these conditions.[31,32] Upon increasing the temperature, the carbonation rate rose sharply due to the transformation to potassium dawsonite, reaching a maximum at 400 K. Above 473 K decomposition of the K-DW phase occurred, with a maximum rate at 573 K, in agreement with the findings of thermogravimetric analysis. The latter also revealed that a small fraction of highly-stable carbonates remains in the structure. Although they could be decomposed by increasing the regeneration temperature, it is kept relatively low (773 K) to prevent the crystallisation of certain aluminium oxides, like α-Al_2O_3, which cannot be reconverted into a dawsonite phase.[33] To confirm the regenerability of the sample under a pressurised pure CO_2 atmosphere, the as-synthesised K-DW was heated to 773 K (5 K min^{-1}) in 3.0 MPa of CO_2. No dawsonite phase remained in the sample isolated after rapid cooling under flowing CO_2 (Fig. S3). This is prerequisite to producing a compressed stream of carbon dioxide for transport or subsequent utilisation.

Finally, the influence of water and CO_2 concentration on the kinetics of dawsonite formation was investigated. Firstly, a linear increase in the net capacity with an ascending molar H_2O/CO_2 ratio was observed (Fig. 4c). This coincides with previous suggestions that the hydroxylation of the calcined material is rate-determining, proceeding through a $K_2(Al_2O(OH)_6)$ intermediate,[35] the formation of which was also detected in our K-DW sorbent (Fig. 3b). Secondly, it was demonstrated that a decrease in the CO_2 concentration is beneficial in terms of net capacity. For this, the feed concentration of both H_2O and CO_2 was lowered from 25 to 12.5 mol.%, balanced by N_2 for keeping the total flow constant The resulting equilibrated net capacity increased from 0.89 to 1.36 mmol g^{-1}. This can be explained by the slower flow of carbon dioxide which in turn results in a longer residence time in the sorbent bed and consequently in an improved conversion into the dawsonite phase. This suggests that the concentration of CO_2 is not a limiting factor; however, a balance must be found between the residence time and the reaction rate of dawsonite formation in order to optimise the dynamic uptake.

3.2 Design of technical dawsonite-based sorbents

A crucial milestone in the development of any prospective CO_2 sorbent is the attainment of structured forms suitable for their industrial implementation. Dedicated characterisation tools are required to rationalise the performance of the resulting bodies,

such as Hg porosimetry to assess the porosity and microscopy techniques capable of spatially resolving the internal organisation.[45] Of the strategies evaluated (Fig. 5), the direct extrusion of the uncalcined K-DW powder was expected to yield a material with a homogeneous distribution and a stoichiometric loading of potassium. However, stable extrudates could not be attained by this route, owing to the poor self-binding properties of the material. On the other hand, extrusion of the mixed oxide phase, derived upon calcination of the K-DW powder, resulted in bodies exhibiting an opaque glassy appearance and negligible porosity (coded B, Table 1). Although subsequent evaluation revealed a virtually identical net CO_2 capacity to that of the powder analogue over multiple cycles (Fig. S4a), examination of the sorbent bed after the fifth carbonation disclosed that the extrudates were largely destroyed (Fig. S4b). The densely-packed structure appeared unable to withstand repeated carbonation and regeneration, suggesting that the interparticle interactions were weakened, for example due to morphological changes.

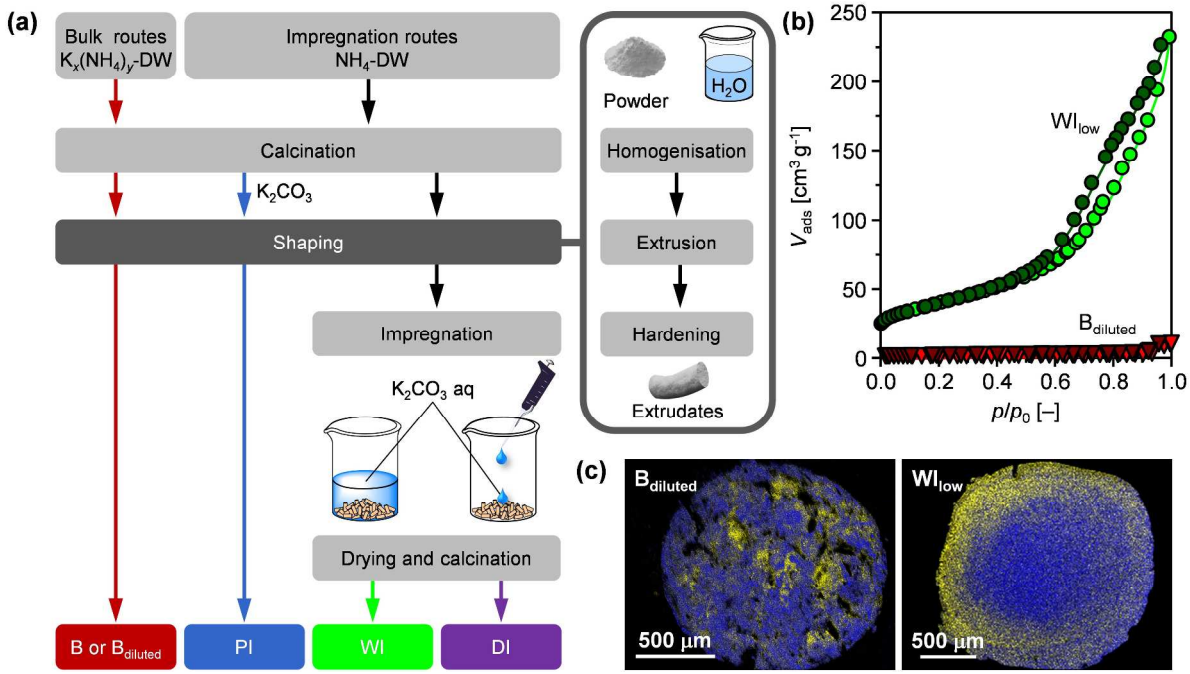

Fig. 5 (a) Strategies to prepare shaped dawsonite-based sorbents: bulk routes involving the direct structuring of calcined K-DW (B) or K(NH_4)-DW ($B_{diluted}$) precursors and impregnation routes incorporating K_2CO_3 by extrusion with γ-Al_2O_3 (PI), or through dry (DI) or wet (WI) impregnation of pre-formed γ-Al_2O_3 bodies. The critical impact of the mode of potassium incorporation is clearly illustrated on comparison by (b) N_2 sorption and (c) EDX mapping (blue: Al, yellow: K); a significantly enhanced porosity was exhibited by the WI_{low} than the $B_{diluted}$ sample, whereas a more eggshell potassium distribution resulted in the impregnated sample.

Since the extent of structural alteration was expected to be linked with the alkali-metal content, we deduced that a potassium-deficient material could exhibit improved stability. In bulk systems, reduced alkali metal loadings can be attained by replacing some of the potassium ions with ammonium during the precipitation, yielding an intimate mixture of K-DW and NH_4-DW. The ammonium dawsonite is subsequently transformed into γ-Al_2O_3 upon calcination resulting in extrudates of alumina-diluted $KAlO_2$-K_2CO_3 (coded $B_{diluted}$). However, despite their lower potassium loading (13 wt.%), the extrudates remained nonporous (Fig. 5b) and still suffered significant loss of mechanical integrity. The development of cracks due to the growth of needle-like crystals was clearly visible in SEM micrographs (Fig. 6a, inset) and was also reflected in an increased total surface area (from <1 to 22 $m^2 g^{-1}$). Interestingly, this sample required a longer equilibration period (4 cycles) than any other system before reaching a stable net uptake (Fig. 6a). EDX analysis of internal cross-sections revealed that the inhomogeneous distribution of potassium in the fresh sample (Fig. 5c) became more uniformly dispersed after 5 cycles (Fig. 6a, inset).

Impregnation routes provide a versatile alternative preparation strategy, permitting facile variation of the potassium content and the application of diverse alumina sources. We believed that by applying a high surface area γ-alumina, derived by the thermal decomposition of NH_4-DW, we could enhance the porosity of the resulting body and thereby maximise the interaction of CO_2 and H_2O with the alkali metal. K_2CO_3 was introduced by three methods; (*i*) during homogenisation of the wet γ-alumina paste prior to shaping (paste impregnation, coded PI), or by (*ii*) the wet (coded WI), or (*iii*) dry (coded DI) impregnation of pre-formed γ-alumina extrudates. Potassium loadings of 13 or 27 wt.% were targeted in each case to enable direct comparison with the diluted and stoichiometric bulk samples, respectively. Lower loading clearly resulted in improved stability, which was attributed to the increased porosity of the resulting extrudates (PI_{low}, WI_{low}, and DI_{low} in Table 1) coupled to the less extensive formation of

the dawsonite phase. However, $q_{net}(CO_2)$ was limited in all cases. In contrast to the diluted bulk sample, equilibration of the impregnated samples occurred within the first cycle (Fig. 6a).

In order to maximise the CO_2 capture capacity, higher K loadings are required. Under these circumstances, wet impregnation was not applicable since the concentrated solution induced the partial dissolution of the extrudates. On the other hand, paste impregnation yielded extrudates (PI_{high}) of similar porosity and low stability to those prepared by bulk routes (Table 1). In contrast, the dry-impregnated samples (DI_{high}) presented almost double the initial meso- and macropore volume and evidenced the lowest fines formation upon testing. In contrast to the large cracks evidenced in PI_{high} after five carbonation cycles, smaller and more dispersed voids were observed in the case of DI_{high} (Fig. 6b). These findings corroborate the crucial importance of the total pore volume (meso- and macroporosity) as a descriptor for the stability of dawsonite-based shaped sorbents. While the potassium availability governs the maximum uptake, as illustrated by the linear correlation between the equilibrated $q_{net}(CO_2)$ and the K

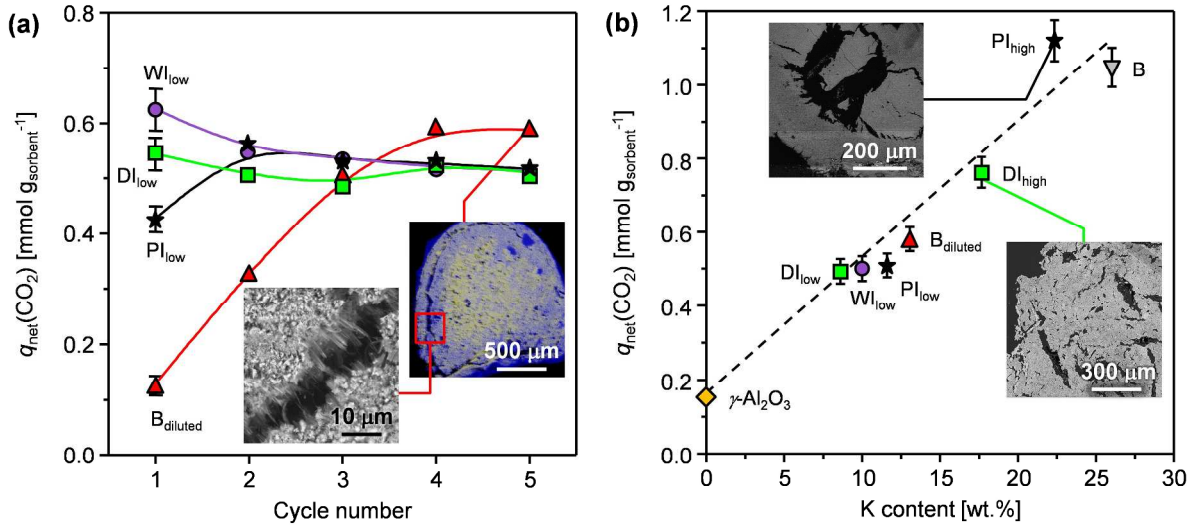

Fig. 6 (a) Net CO_2 capacity of potassium dawsonite-based sorbents prepared by different routes. The EDX overlay inset highlights the distribution of K (yellow) and Al (blue) after 5 cycles, while the SEM image reveals the extensive growth of needle-like dawsonite crystals at the interface of large cracks. (b) Relation between the K content and the net CO_2 capacity of the shaped sorbents after 5 cycles. The performance of the pure γ-alumina extrudates is shown for reference. The SEM micrographs inset reveal the high density of cracks appearing in the DI_{high} and PI_{high} sorbents. Reaction conditions as detailed in Fig. 2.

content (Fig. 6b), comparison of the breakthrough curves of DI_{high} and PI_{high} reveals that the carbonation kinetics were strongly affected by the extrudate porosity (Fig. S5). In particular, a reduced rate of surface reaction was observed for the latter, in line with the lower pore volume and total surface area.

To understand the structural evolution upon consecutive carbonation and regeneration, the dry-impregnated sorbent with high K loading was visualised by microscopy at different stages of the life cycle (Fig. 7a, top row). Consistent with the variation observed in $B_{diluted}$, the initial eggshell distribution of potassium in the shaped body was altered in successive cycles. The migration of potassium ions is in line with their reportedly high mobility at high pressure in the presence of steam,[35] and is correlated with the equilibration period in the net capacity (Fig. 7b). Furthermore, the potassium enrichment visible along cracks in the carbonated sample indicates that the alkali metal preferentially accumulates along these pathways, which suggests that the crack formation is associated with the growth of dawsonite crystals. This was further corroborated by comparison of the TEM images (Fig. 7a, bottom row), in which the change in particle morphology is clearly distinguished.

Assessment of the variation in the porous properties of samples isolated after each carbonation and regeneration step over ten cycles by Hg porosimetry (Fig. 8a), evidences how the

Table 1 Characterisation data and net CO_2 uptake of dawsonite-based extrudates.

Sample	Potassium[a] [wt.%]	S_{BET}[b] [$m^2\ g^{-1}$]	V_{macro}[c] [$cm^3\ g^{-1}$]	V_{meso}[c] [$cm^3\ g^{-1}$]	ρ_{Hg}[d] [$g\ cm^{-3}$]	$q_{net}(CO_2)$[e] [mmol g_K^{-1}]
B	27	<1	–	–	–	4.01
$B_{diluted}$	13	<1	–	–	–	3.81
γ-Al_2O_3	–	257	0.20	0.26	1.24	–
PI_{low}	12	36	0.08	0.06	1.90	4.23
PI_{high}	24	22	0.05	0.05	3.69	4.96
WI_{low}	10	130	0.24	0.24	1.20	5.00
DI_{low}	9	109	0.11	0.29	1.36	5.60
DI_{high}	19	65	0.13	0.12	1.75	4.06
DI_{high}-a[f]	13	152	0.24	0.29	1.10	3.83
DI_{high}-s[g]	16	36	0.28	0.06	1.47	4.49

[a] ICP-OES. [b] BET method. [c] Determined from the amount of Hg intruded into pores of 3.0–50 nm (V_{meso}) or >50 nm (V_{macro}) in diameter, respectively. [d] Bulk density determined by Hg porosimetry. [e] Fifth carbonation. [f] Attapulgite (10 wt.%) which is converted into a mixed metal oxide upon calcination. [g] Starch (10 wt.%) which is removed from the extrudates by calcination.

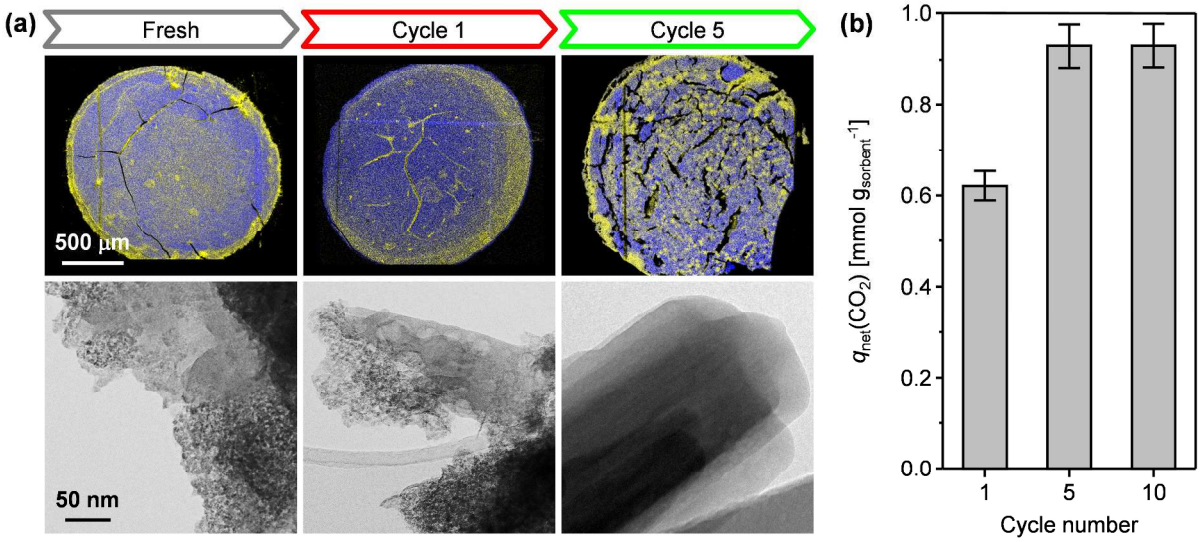

Fig. 7 (a) EDX maps of the potassium (yellow) and aluminium (blue) distribution in extrudate cross-sections of the fresh dry-impregnated sorbent DI_{high} (19 wt.% potassium) and after carbonation in the cycle indicated (top row). TEM examination of the particle morphology in the corresponding crushed extrudates (bottom row). The scale bars shown on the left apply to all images in the same row. (b) Corresponding net CO_2 capacity. Reaction conditions as detailed in Fig. 2.

growing crystals initially fill the interparticle pore volume, but then as they collide with the surrounding matrix they lead to an increased macropore volume as µm-sized cracks form (Fig. S6) and the extrudates break apart. During regeneration, the mesopore volume can be partially regained; however, the swelling gradually continues until the 5th cycle after which the bulk density remains constant (Fig. 8a).

3.3 Stabilising role of additives in dawsonite-based sorbents

Having demonstrated the obtainment of relatively stable dawsonite systems *via* the dry impregnation of a high surface area γ-alumina, we evaluated the potential of two strategies to prevent attrition of the sorbents: (*i*) the generation of supplementary void volume to better accommodate morphological changes within the shaped body through the application of pore formers, and (*ii*) the use of inorganic binders to provide a reinforcing matrix in which K_2CO_3-$KAlO_2$-γ-Al_2O_3 is embedded.[39]

Additives applied as sacrificial pore formers are typically cheap materials, such as starch or carbon black. As these materials are thermally decomposed during the hardening step following extrusion, they are not expected to impact the CO_2

capacity of the technical sorbent. Since the strength of the shaped body is correlated with the void fraction, this limits the amount of pore former which can be applied. Here, mechanically-stable γ-alumina extrudates with a 60% increased total pore volume could be obtained on application of 10 wt.% (dry weight) of a commercial corn starch. Furthermore, although the porosity was reduced following the dry impregnation of K_2CO_3 ($DI_{high\text{-}s}$, Table 1), it remained 20% higher that of the DI_{high} sample. Comparatively, $DI_{high\text{-}s}$ exhibited a higher equilibrated $q_{net}(CO_2)$ per gram of potassium than DI_{high} (4.49 mmol g_K^{-1} with respect to 4.06 mmol g_K^{-1}), indicating that the increased accessibility led to a more efficient utilisation of the alkali metal. However, the formation of fines in the sorbent bed after multiple cycles disclosed that the effect of the pore former was insufficient to prevent long-term degradation of the shaped bodies.

An alternative strategy to enhance the stability is to exploit permanent inorganic binders, since they remain as a continuous network in the extrudate serving as a rigid matrix for the reactive phase while preferably not interfering with the sorption properties. Refractory aluminas, silicas, and clays materials are commonly applied due to their high stability and natural abundance. Depending on the particle properties (size and morphology) of the binder, they may also enhance the intrinsic pore volume of the shaped body. Since clays often features large particle sizes, we studied the incorporation of a commercial attapulgite clay.

In this case the optimal amount of 10 wt.% of binder was determined by the balance between improving the mechanical strength and maximising the sorption capacity. The attapulgite containing extrudate exhibited a 25% enhanced porosity, which was almost completely preserved upon impregnation ($DI_{high\text{-}a}$, Table 1). The huge impact of the binder, keeping the porous network intact over five cycles, can be seen from the pore size distribution (Fig. 8b). All pores larger than 10 nm are preserved upon carbonation and smaller pores are only partially filled compared to DI_{high}, where the porous network entirely collapsed over the five cycles. Closer examination by FIB-SEM reveals that the binder is intimately mixed with the dawsonite phase in the carbonated sample (Fig. 8c, bottom). The interwoven matrix formed by the binder evidently does not inhibit the growth of dawsonite crystals, but appears to support the macrostructure of $DI_{high\text{-}a}$ by providing a flexible network which prevents formation of the large cracks visible in DI_{high} (Fig. 8c, top).

Despite these benefits, the attapulgite-containing sorbent exhibits a slightly lower $q_{net}(CO_2)$ (3.83 mmol g_K^{-1}) to those evidenced for the samples prepared with starch or in the absence

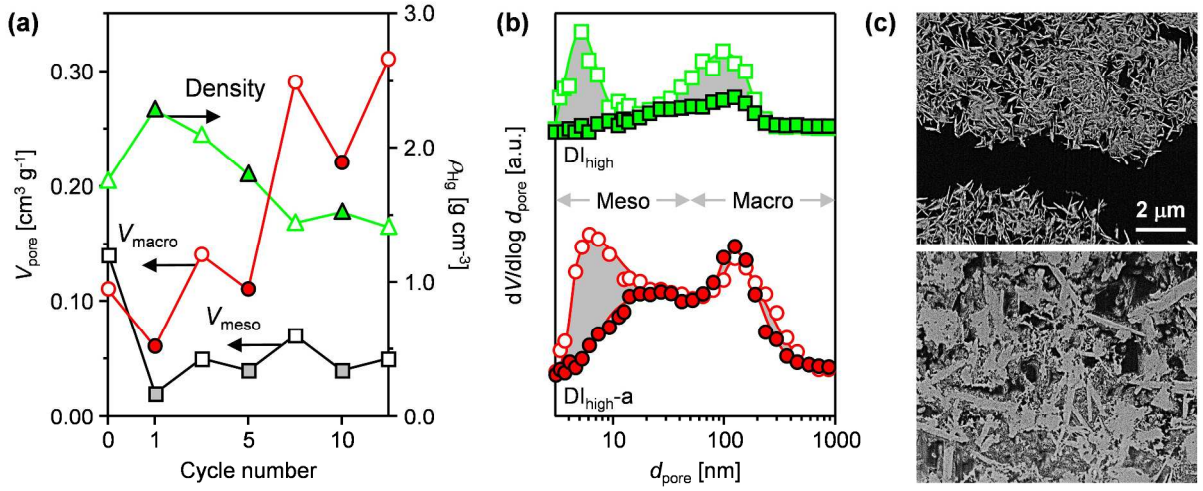

Fig. 8 (a) Porous properties and density derived by Hg intrusion of the carbonated (solid symbols) and regenerated (open symbols) dry-impregnated extrudates (DI_{high}) after the 1st, 5th, and 10th cycle. The fresh sorbent is shown at 0. (b) Pore-size distributions of the fresh (open symbols) and carbonated (5th cycle, solid symbols) binder-free and binder-containing dry-impregnated extrudates (DI_{high}-a). Shaded areas indicate the difference in pore volume. (c) Corresponding FIB-SEM micrographs of the carbonated DI_{high} (top) and DI_{high}-a (bottom) samples. The scale bar applies to both images.

of pore former/binder, respectively. This was unexpected since EDX maps of internal cross-sections confirmed a favourable eggshell distribution of potassium within the sample (Fig. S7a). However, the formation of a boehmite phase AlO(OH) was detected after the 5th carbonation (Fig. S7b), indicating that a minor fraction of potassium is unavailable for dawsonite formation, which is corroborated by the much lower total capacity of $DI_{high\text{-}a}$ with respect to DI_{high} (3.85 *vs.* 10.53 mmol g_K^{-1}). Presumably the boehmite side phase forms in K-deficient regions of the sample, which could result from the preferential deposition of potassium on the matrix. However, regardless of the slightly reduced efficiency, the continuous binder network formed within $DI_{high\text{-}a}$ yielded the highest mechanical stability of all the shaped sorbents, with no loss of fines observed after ten consecutive cycles. Thus, the application of a binder enables the optimal combination of high and stable CO_2 net uptakes, fast carbonation kinetics, and excellent durability.

Despite the valuable features of K-DW-based sorbents demonstrated in this work, future studies also need to consider

long-term performance over hundreds of cycles, heat management, process engineering and cost evaluation of the capture process. This techno-economic analysis is beyond the scope of this work and will enable to draw conclusions on the large-scale feasibility of the system.

5 Conclusions

This study has demonstrated the strong potential of dawsonite-based systems for carbon capture at moderate temperature (473 K) and pressure (3.0 MPa) conditions. Potassium dawsonite was shown to have double the net capacity of sodium dawsonite or of the hydrotalcite benchmark, due to the irreversible formation of Na_2CO_3 or to the hindered reconstruction of the mixed Mg-Al oxides, respectively. Comparison of the performance under different conditions confirmed the enhanced uptake in the presence of steam deriving from the requirement of H_2O for the crystallisation of the dawsonite phase. Furthermore, the sorbent was regenerable in carbon dioxide atmospheres at elevated pressure, demonstrating the possibility to derive pure CO_2 streams from the capture process.

The implications of material scale up have been highlighted through the characterisation and evaluation of shaped potassium dawsonite-based extrudates prepared *via* different methodologies. High loadings and eggshell distributions of potassium combined with a well-developed meso- and macropore network were found to be crucial to obtain hydrothermally-stable sorbents with fast carbonation kinetics and high CO_2 capacity. Of the routes studied, the dry impregnation of γ-alumina bodies offered the greatest flexibility to merge these characteristics. The utilisation of binders, and to some extent pore formers, was indispensable to maintain mechanical stability upon the carbonation–regeneration cycles, preventing the loss of large pores. The approach demonstrated herein for the transition from powder to technical body is applicable to any other sorbent, representing the key value of this contribution.

Acknowledgements

The authors acknowledge the Swiss Federal Institute of Technology ETHZ for funding, the Scientific Center for Optical and Electron Microscopy ScopeM for use of their facilities, Dr. Karsten Kunze for support with SEM measurements, Stephan Handschin for help with specimen preparation, and Nina-Luisa Michels for conducting FIB-SEM imaging.

Notes and references

1 International Energy Agency, in *World Energy Outlook 2013*, 2013, London, UK.
2 K. M. K. Yu, I. Curcic, J. Gabriel and S. C. E. Tsang, *ChemSusChem*, 2008, **1**, 893.
3 M. E. Boot-Handford, J. C. Abanades, E. J. Anthony, M. J. Blunt, S. Brandani, N. Mac Dowell, J. R. Fernández, M.-C. Ferrari, R. Gross, J. P. Hallett, R. S. Haszeldine, P. Heptonstall, A. Lyngfelt, Z. Makuch, E. Mangano, R. T. J. Porter, M. Pourkashanian, G. T. Rochelle, N. Shah, J. G. Yao and P. S. Fennell, *Energy Environ. Sci.*, 2014, **7**, 130.
4 E. V. Kondratenko, G. Mul, J. Baltrusaitis, G. O. Larrazábal and J. Pérez-Ramírez, *Energy Environ. Sci.*, 2013, **6**, 3112.
5 Global CCS Institute, in *The Global Status of CCS*, 2014, Docklands, Australia.
6 D. M. D'Alessandro, B. Smit and J. R. Long, *Angew. Chem., Int. Ed.*, 2010, **49**, 6058.
7 G. T. Rochelle, *Science*, 2009, **325**, 1652.
8 S. D. Sharma and M. Azzi, *Fuel*, 2014, **121**, 178.
9 N. Mac Dowell, N. Florin, A. Buchard, J. Hallett, A. Galindo, G. Jackson, C. S. Adjiman, C. K. Williams, N. Shah and P. Fennell, *Energy Environ. Sci.*, 2010, **3**, 1645.
10 A. Samanta, A. Zhao, G. K. H. Shimizu, P. Sarkar and R. Gupta, *Ind. Eng. Chem. Res.*, 2012, **51**, 1438.
11 S. Choi, J. H. Drese and C. W. Jones, *ChemSusChem*, 2009, **2**, 796.
12 Q. Wang, J. Luo, Z. Zhong and A. Borgna, *Energy Environ. Sci.*, 2011, **4**, 42.
13 J. C. Hicks, J. H. Drese, D. J. Fauth, M. L. Gray, G. Qi and C. W. Jones, *J. Am. Chem. Soc.*, 2008, **130**, 2902.
14 G. Qi, Y. Wang, L. Estevez, X. Duan, N. Anako, A.-H. A. Park, W. Li, C. W. Jones and E. P. Giannelis, *Energy Environ. Sci.*, 2011, **4**, 444.
15 Y.-S. Bae and R. Q. Snurr, *Angew. Chem., Int. Ed.*, 2011, **50**, 11586.
16 K. Sumida, D. L. Rogow, J. A. Mason, T. M. McDonald, E. D. Bloch, Z. R. Herm, T.-H. Bae and J. R. Long, *Chem. Rev.*, 2012, **112**, 724.
17 R. Banerjee, A. Phan, B. Wang, C. Knobler, H. Furukawa, M. O'Keeffe and O. M. Yaghi, *Science*, 2008, **319**, 939.
18 T.-H. Bae, M. R. Hudson, J. A. Mason, W. L. Queen, J. J. Dutton, K. Sumida, K. J. Micklash, S. S. Kaye, C. M. Brown and J. R. Long, *Energy Environ. Sci.*, 2013, **6**, 128.
19 T. L. P. Dantas, F. M. T. Luna, I. J. Silva Jr., D. C. S. de Azevedo, C. A. Grande, A. E. Rodrigues and R. F. P. M. Moreira, *Chem. Eng. J.*, 2011, **169**, 11.
20 D. Qian, C. Lei, E.-M. Wang, W.-C. Li and A.-H. Lu, *ChemSusChem*, 2014, **7**, 291.
21 G. Majano, O. Martin, M. Hammes, S. Smeets, C. Baerlocher and J. Pérez-Ramírez, *Adv. Funct. Mater.*, 2014, DOI:10.1002/ adfm.201303678.
22 J. C. Abanades, E. S. Rubin and E. J. Anthony, *Ind. Eng. Chem. Res.*, 2004, **43**, 3462.
23 J. Blamey, E. J. Anthony, J. Wang and P. S. Fennell, *Prog. Energy Combust. Sci.*, 2010, **36**, 260.
24 A. M. Kierzkowska, R. Pacciani and C. R. Müller, *ChemSusChem*, 2013, **6**, 1130.
25 P. Sun, J. R. Grace, C. J. Lim and E. J. Anthony, *AIChE J.,* 2007, **53**, 2432.
26 M. Broda and C. R. Müller, *Adv. Mat.*, 2012, **24**, 3059.
27 J. R. Hufton, S. Mayorga and S. Sircar, *AIChE J.*, 1999, **45**, 248.
28 N. N. A. H. Meis, J. H. Bitter and K. P. de Jong, *Ind. Eng. Chem. Res.*, 2010, **49**, 8086.
29 M. K. Ram Reddy, Z. P. Xu, G. Q. Lu and J. C. Diniz da Costa, *Ind. Eng. Chem. Res.*, 2008, **47**, 2630.

30 N. N. A. H. Meis, A. M. Frey, J. H. Bitter and K. P. de Jong, *Ind. Eng. Chem. Res.*, 2013, **52**, 12812.
31 S. C. Lee, B. Y. Choi, T. J. Lee, C. K. Ryu, Y. S. Ahn and J. C. Kim, *Catal. Today*, 2006, **111**, 385.
32 S. C. Lee, Y. M. Kwon, C. Y. Ryu, H. J. Chae, D. Ragupathy, S. Y. Jung, J. B. Lee, C. K. Ryu and J. C. Kim, *Fuel*, 2011, **90**, 1465.
33 G. Stoica and J. Pérez-Ramírez, *Chem. Mater.*, 2007, **19**, 4783.
34 G. Stoica, J. C. Groen, S. Abelló, R. Manchanda and J. Pérez-Ramírez, *Chem. Mater.*, 2008, **20**, 3973.
35 S. Walspurger, P. D. Cobden, W. G. Haije, R. Westerwaal, G. D. Elzinga and O. V. Safonova, *Eur. J. Inorg. Chem.*, 2010, **2010**, 2461.
36 O. Aschenbrenner, P. McGuire, S. Alsamaq, J. Wang, S. Supasitmongkol, B. Al-Duri, P. Styring and J. Wood, *Chem. Eng. Res. Des.*, 2011, **89**, 1711.
37 E. L. G. Oliveira, C. A. Grande and A. E. Rodrigues, *Sep. Purif. Technol.*, 2008, **62**, 137.
38 M. Maroño, Y. Torreiro and L. Gutierrez, *Int. J. Greenhouse Gas Control*, 2013, **14**, 183.
39 S. Mitchell, N.-L. Michels and J. Pérez-Ramírez, *Chem. Soc. Rev.*, 2013, **42**, 6094.
40 F. Cavani, F. Trifirò and A. Vaccari, *Catal. Today*, 1991, **11**, 173.
41 H.-J. Bart and U. von Gemmingen, in *Ullmann's Encyclopedia of Industrial Chemistry*, Wiley-VCH Verlag GmbH & Co. KGaA, Weinheim, 7th edn, 2012, vol. 1, p. 552.
42 N. D. Hutson, S. A. Speakman and E. A. Payzant, *Chem. Mater.*, 2004, **16**, 4135.
43 Y. Gao, Z. Zhang, J. Wu, X. Yi, A. Zheng, A. Umar, D. O'Hare and Q. Wang, *J. Mater. Chem. A*, 2013, **1**, 12782.
44 M. K. Ram Reddy, Z. P. Xu, G. Q. Lu and J. C. Diniz da Costa, *Ind. Eng. Chem. Res.*, 2006, **45**, 7504.
45 S. Mitchell, N.-L. Michels, K. Kunze and J. Pérez-Ramírez, *Nat. Chem.*, 2012, **4**, 825.

Broader context

Capturing CO_2 from large-point sources is regarded as a vital milestone for the abatement of rising greenhouse gas emissions related to the continuing role of fossil-fuelled power stations in the global energy mix. In the immediate term, retrofitting a capture unit to an existing power plant necessitates the use of hydrothermally-stable sorbents due to the elevated steam concentration in the flue gas. While the current amine-scrubbing process demonstrates high recovery rates, energy penalties associated with sorbent regeneration, equipment corrosion, solvent degradation, and reagent disposal remain far from optimal. Although several physi- and chemisorbent systems, such as zeolites, MOFs, CaO, alkali bicarbonates, and hydrotalcites, are known to exhibit promising CO_2 uptakes under specific conditions, the potential of dawsonite-based sorbents has been overlooked. Moreover, few fundamental studies have been devoted to understanding the technical development of these solid systems. For this purpose, chemical transformations originating reversible high CO_2 capacity at the atomic scale must be confronted with meso- and macroscale considerations of scale up and process engineering. We illustrate herein key challenges in the preparation of mechanically-stable dawsonite-based materials in extrudate form and demonstrate their thriving CO_2 capture performance, which is unrivalled in the presence of steam.